

Detection, sky localization and early warning for binary neutron star mergers by detectors located in China of different configurations in third generation detector network

YUFENG LI

*School of Physics and Technology, Wuhan University, Wuhan 430072, China and
SUPA, School of Physics and Astronomy, University of Glasgow, Glasgow G12 8QQ, United Kingdom*

Ik Siang Heng

SUPA, School of Physics and Astronomy, University of Glasgow, Glasgow G12 8QQ, United Kingdom

Man Leong Chan*

Department of Physics and Astronomy, The University of British Columbia, Vancouver, BC V6T 1Z4, Canada

XILONG FAN†

School of Physics and Technology, Wuhan University, Wuhan 430072, China

Lijun Gou

*Key Laboratory for Computational Astrophysics, National Astronomical Observatories,
Chinese Academy of Sciences, Beijing 100101, China and
School of Astronomy and Space Science, University of Chinese Academy of Sciences, Beijing 100049, China*

This work shows the results of an evaluation of the impact that a detector located in China, with a noise budget comparable to that of a proposed high-frequency detector with a 20 km arm length, an Einstein Telescope (ET) or a Cosmic Explorer (CE), could have on the network of ET-CE in terms of detection rate, localization, and providing early warning alert for simulated binary neutron star (BNS)s. The results indicate that a three-detector network including a Chinese detector could identify at least 4.4% more BNS mergers than an ET-CE network alone. The localization uncertainty could be reduced by a factor of more than 5 on average compared to the ET-CE network. With a three-detector network involving a Chinese detector, up to 89% of BNS mergers could be located within 10 square degrees of the sky 10 minutes prior to the merger. The assessment suggests that the potential for early warning signals is highest when the Chinese detector is similar to ET, whereas the sources are detected with the highest signal-to-noise ratio and localized to the smallest regions when the detector is more akin to CE. Interestingly, the C20N network (comprising ET+CE+C20) can achieve comparable localization performance as the ET network while outperforming the ETCN network (featuring the ET+CE+ an ET-like detector in China) in terms of detection capabilities, especially at large distances, indicating that adding a 20 km kilohertz detector in China to ET-CE network would make significant contributions at least as adding an ET-like detector in China to multi-messenger astronomy for almost all BNS observations.

I. INTRODUCTION

Two years after the first detection of gravitational wave (GW) on September 14, 2015 [[1–3]], a GW signal from a binary neutron star inspiral was observed by Advanced LIGO and Advanced Virgo on August 17, 2017, leading to the first-ever joint detection of gravitational and electromagnetic radiation from a single source [6]. The identification of the correlated gamma-ray burst by [19], along with the subsequent electromagnetic (EM) follow-up campaign, heralded the era of multi-messenger astronomy, synergized with GWs [6]. The case of GW170817 [6] demonstrated the tremendous scientific potential of successfully observing the associated EM counterparts of a

GW event. Observing an EM counterpart offers several advantages. Establishing a link between the GW trigger and its progenitor can yield valuable insights into the progenitor and its surrounding environment [12, 16, and 23]. Moreover, independently measuring the redshift of the source emitting the GW signal via the observation of an EM counterpart facilitates cosmological examinations and constraining the equation of state of dark energy [4, 36, and 37]. Hence, comprehending how to optimize the combined efficiency of GWs and their corresponding electromagnetic counterparts is crucial for maximizing scientific advancements.

Localization uncertainty and early warning capability (the ability to detect signals prior to mergers with reasonable localization uncertainty [14]) are pivotal factors directly influencing the effectiveness of combined gravitational wave (GW) and electromagnetic (EM) observations. Second-generation detectors like Advanced LIGO [26], operating at their design sensitivity, are pro-

* mervync@phas.ubc.ca

† xilong.fan@whu.edu.cn

jected to detect only 10^{-5} of all binary neutron star (BNS) mergers. Moreover, the median sky localization area (90% credible region) for compact binary coalescences during the third observation run of the LIGO and Virgo collaborations was a few hundred square degrees [10][7]. Therefore, the sensitivity of current-generation detectors is constrained in their capacity to conduct a substantial number of GW-EM joint observations. However, with the emergence of third-generation detectors such as the Einstein Telescope (ET) [29], a proposed underground detector in Europe (more details available on the ET website(<http://www.et-gw.eu>), and the Cosmic Explorer (CE) [32], a planned next-generation GW observatory in the United States(<https://cosmicexplorer.org>), BNS detection rates could improve by up to 3-4 orders of magnitude [13, 20]. These detectors are expected to detect about 50% of all BNS mergers and localize the majority of them to $\leq 200\text{Mpc}$ with uncertainties of $\mathcal{O}(1)\text{deg}^2$, and $\leq 100\text{deg}^2$ for most BNS mergers $\leq 1600\text{Mpc}$, as reported by [15]. By incorporating a third detector into the network comprising ET-CE, the angular resolution of gravitational wave events will experience a significant enhancement. This enhancement stems from the fact that the localization uncertainty is inversely proportional to the area enclosed by the three detectors [38]. Consequently, a larger area encompassed by the three detectors is favored to minimize localization errors for the three-detector network.

Recent research has investigated the potential of incorporating a detector in Australia into the ET-CE network, as proposed in studies by [11, 18, 22, and 34]. In a similar vein, as detailed in our previous work [25], we investigated the detection capabilities, localization uncertainty, and early warning performance of a three-detector network (comprising ET, CE, and a comparable detector in Australia) during the third-generation detector era for BNS mergers. We discovered that the extensive baseline between these detectors enabled the localization of the majority of sources within 0.25deg^2 up to distances of 200 Mpc. Moreover, the prolonged in-band duration enabled by third-generation detectors could facilitate the accumulation of sufficient signal-to-noise ratio for a potential GW signal to achieve statistical significance before the merger occurs. Consequently, this could improve the likelihood of early warning and subsequent EM follow-up observations.

Based on the preceding discussion, it becomes evident that establishing a global network of gravitational wave detectors, especially in diverse geographic locations, is a crucial step towards enhancing the precision of gravitational wave source localization. Given our interest in China's contributions to the field of gravitational wave localization, it's worth noting that its geographic location could create a vast triangular area with Europe and the United States. This positioning holds the potential to significantly augment both the detection rate and localization accuracy when compared to the ET-CE network.

Therefore, assessing the performance of gravitational

wave detectors in China serves not only the demands of scientific inquiry but also the advancement of technological innovation and high-tech sectors within China. Additionally, it fosters collaboration and growth in global scientific research endeavors. Motivated by these considerations, our objective is to examine the detection capabilities, localization accuracy, and early warning efficacy of a three-detector network comprising third-generation GW detectors—namely ET, CE, and a comparable detector in China—for BNS mergers. This assessment aims to gauge the contribution of Chinese detectors to the global GW detector network in advance. Such insight is crucial for determining whether China should establish a ground-based GW detector in the future and what configuration would be most advantageous for localization efforts.

Prior studies conducted by [22] and [34] have investigated the influence of a hypothetical detector in China on the network's capacity to localize gravitational wave sources. Utilizing three Figures of Merit—reconstruction polarization capability, localization accuracy, and parameter accuracy—they concluded that the southern region of China would offer improved performance when integrated into a network comprising advanced LIGO Hanford, advanced LIGO Livingston, advanced Virgo, and KAGRA. We have chosen Wuhan (30.52°N , -114.30°E) in Hubei province as the testing ground for our virtual GW detectors. Its central position in China, far from coastal areas and seismic zones, along with its flat terrain and stable underground structures, render it an optimal site for ground-based detector. These attributes reduce the influence of earthquakes and environmental noise on the detectors, thereby enhancing their sensitivity and therefore localization accuracy. Moreover, the Wuhan city government is capable of providing ample land for constructing a GW detector. Furthermore, Wuhan's suitability has previously been evaluated for its potential to constrain string cosmology in a study by [24]. Our assessment of its localization performance will provide additional insights into the feasibility of Wuhan as a prospective site for a future ground-based gravitational wave detector in China.

In China, there have been ongoing discussions regarding the configuration of potential future ground-based detectors, with one particularly unique proposal being the kilohertz detector. Distinguished by its exceptional sensitivity at kilohertz frequencies, this detector is poised to bridge the gap for future gravitational wave detection within this frequency range. Notably, it holds the promise of observing neutron star post-merger oscillations—an occurrence arising from the energy released during neutron star mergers, which induces high-frequency oscillations in the resulting remnant [28]. Kilohertz detectors possess the capability to detect and analyze these oscillations, thereby furnishing invaluable insights into the properties and structure of neutron stars, the equation of state of nuclear matter, and the remnant's role as the central engine for energetic electromagnetic

emissions. [27] suggested that an optimal arm length of approximately 20 km is necessary for observing neutron star post-merger oscillations. To assess the viability of establishing such a 20 km kilohertz detector in China in the future, various aspects of the detector’s performance need consideration, including sensitivity, economic and technical feasibility, signal-to-noise ratio, and localization accuracy. In our previous work [24], we evaluated the constraining capability of a 20 km detector in Wuhan for string cosmology. Furthermore, assessing the localization accuracy of a 20 km detector in Wuhan will further inform the discussion on whether China should proceed with establishing such a kilohertz detector.

By simulating a 20 km kilohertz detector (hereafter referred to as C20) in Wuhan, forming part of the C20N network (comprising ET+CE+C20, as detailed in Table I), we conducted tests to evaluate the network’s performance and compared it with the ET-CE network. Our study aims to uncover the added value of including C20 in terms of localization performance compared to the ET-CE network. Furthermore, to delve deeper into the influence of various configurations on localization capability in Wuhan, we performed simulations of two additional detectors—an ET-like detector (ET-C) and a CE-like detector (CE-C). Consequently, two testing networks (ETCN: ET-C+ET+CE; CECN: CE-C+ET+CE) were established by combining these simulated detectors with ET and CE, as outlined in Table I.

Moreover, we utilized the same sources as in [25], facilitating a direct quantitative comparison of detection rates, localization accuracy, and early warning performance between deploying the third detector in Australia and China. These sources comprise BNS mergers at fixed distances (100 sources each at 40 Mpc, 200 Mpc, 400 Mpc, 800 Mpc, and 1600 Mpc) and BNS mergers following an assumed astrophysical population (500 sources with a delay time distribution) up to a redshift of ≤ 2 . The information regarding our simulated sources is outlined in Table VII, while the redshift distribution of BNS mergers, following a delay time distribution, is depicted in Figure 6. We adopt the same methodology as employed in [25], which involves calculating signal to noise ratio (SNR) and localization uncertainty using the Fisher Matrix. In the interest of brevity, our focus remains on presenting the results and comparing them with previous findings. For more comprehensive insights into the methods and simulated sources, please refer to [25].

This paper is organized as follows. Section II presents the basic information of third-generation ground-based detectors. Section III presents the results of our analysis. In Section IV, we discuss our findings and provide concluding remarks.

II. THIRD GENERATION DETECTOR

As of the conclusion of their third observing run, Advanced LIGO and Advanced Virgo collectively de-

tected 90 compact binary coalescences, as documented in [8]. These detections carry significant implications for our comprehension of compact binary coalescences and cosmology. Nevertheless, current ground-based detectors are not without limitations, prompting proposals to enhance sensitivity and discover more sources with third-generation ground-based GW detectors projected for the 2030s. The two primary designs for these third-generation GW observatories are CE and ET. The CE design mirrors the current second-generation GW detectors, featuring an L-shaped configuration housing a single interferometer with extended arm lengths of up to 40 km, as delineated in [5] and [17]. Conversely, the proposed ET comprises an underground infrastructure incorporating three interferometers with arm lengths of 10 km, arranged in an equilateral triangular configuration, as elaborated in [21].

Figure 1 depicts the sensitivity curves, expressed as the amplitude spectral density (ASD) as a function of frequency, for ET, CE, and C20. Notably, ET showcases superior sensitivity in the low-frequency band ($< \sim 9$ Hz) compared to CE. This enhancement primarily stems from the substantial reduction of thermal noise achieved by operating the mirrors at cryogenic temperatures as low as 10K [9 and 30]. The heightened low-frequency sensitivity of ET enables earlier detection of inspiralling GW sources and the potential for more early warning alerts. With its significantly longer arm length, CE offers markedly better sensitivity than the other two detectors across nearly the entire frequency band (10 Hz - 1000 Hz), thereby greatly enhancing its ability to explore the depths of the universe and enabling it to detect more sources compared to ET. On the other hand, C20 exhibits excellent sensitivity in the high-frequency band (> 1000 Hz) and comparable sensitivity to ET in the frequency range of approximately 15 Hz to 1000 Hz. Beyond 1 kHz, the sensitivity of GW detectors is typically influenced by the combination of quantum shot noise and classical noises, such as coating thermal noise and gas phase noise. To address these constraints and bolster sensitivity beyond 1 kHz, [27] recommended augmenting input power and introducing squeezed states of light, thereby proposing the concept of a 20 km high-frequency detector. The heightened sensitivity of the 20 km detector in this frequency range proves advantageous for detecting post-merger phases of BNS mergers and holds potential for achieving commendable localization performance, particularly at the time of the merger. Nonetheless, the sensitivity of the 20 km detector experiences a pronounced decline below 15 Hz, limiting its capacity to detect inspiralling GW sources at earlier stages, a capability where ET excels.

The sensitivity of a gravitational wave (GW) detector to an astrophysical source hinges on two key factors: its sensitivity across frequencies, quantified by its amplitude spectral density, and its antenna pattern, which is contingent upon the detector’s geographical position, arm configuration, and the angle between its arms. References

	China (-245.69°E, 30.52°N)	LIGO Hanford (-119.41°E, 46.45°N)	Italy (10.4°E, 43.7°N)
ETCN	ET-C	CE	ET
CECN	CE-C	CE	ET
C20N	C20	CE	ET

TABLE I. Tested networks in this paper, the first column represents the abbreviation for network, where N represents a network. Three kinds of detectors located in China, respectively an ET-like detector (ET-C), a CE-like detector (CE-C), and a high-frequency detector (C20) is assumed to operate with ET and CE to form a three-detector network.

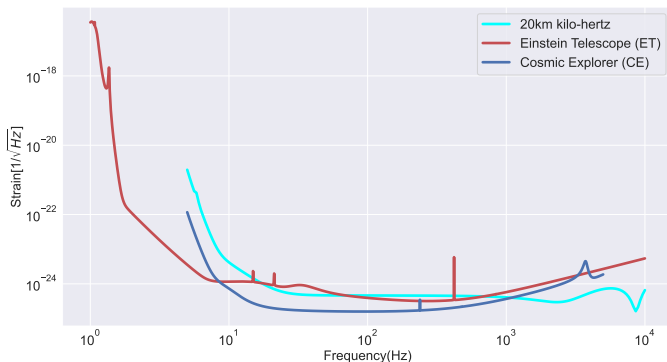


FIG. 1. The amplitude spectral density against frequency for the Einstein Telescope (ET), Cosmic Explorer (CE), and 20 km kilohertz detector.

such as [31] and [25] provide details on the antenna patterns for both the L-shaped detectors (CE, CE-C, C20) and the equilateral triangular-shaped detectors (ET, ET-C). Moreover, for the three virtual detectors situated in Wuhan (ET-C, CE-C, and C20), we adopted the same arm orientation as KAGRA, as done previously in [24]. This choice is supported by studies such as [33], which indicate that the localization criterion is not significantly impacted by the orientation angle of the detector.

III. RESULTS

A. Simulation I: BNS mergers following delay time distribution

1. Detection rates

The optimal signal-to-noise ratio (SNR) (details see Eq(11) of [25]) for 500 simulated sources, as observed by gravitational wave (GW) detector networks listed in Table I, has been calculated. Assuming a network SNR of no less than 8 for a source to be detectable, the analysis reveals detection rates of 91.4%, 98%, 92.2%, and 87% for sources by the ETCN, CECN, C20N, and ET-CE networks, respectively, as summarized in the second row of Table II. Furthermore, the table presents results for the ET-CE network combined with either a CE-like

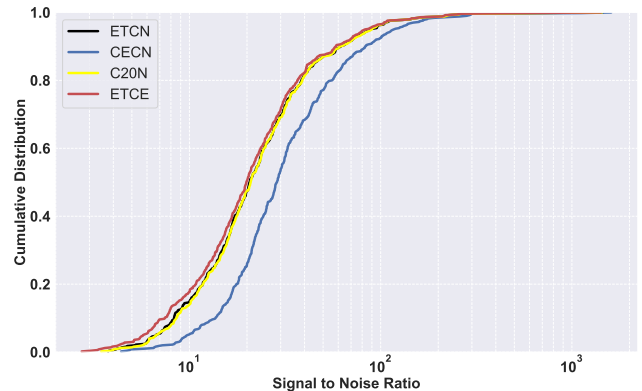


FIG. 2. The cumulative distribution of SNR of tested three detector network configurations and also ET-CE network for the BNSs in Simulation I.

detector in Australia (1ET2CE) or an ET-like detector in Australia (2ET1CE), showcased in the last two columns. These findings are derived using the same sources as those examined in [25], facilitating a direct comparison of the outcomes.

We observed that the inclusion of a detector in China resulted in a minimum of 4.4% more detectable sources compared to the ET-CE network. Among the three detector networks incorporating a Chinese detector, the CECN network exhibited superior performance in source detection compared to the other two networks, while the C20N network, overall, detected 0.8% more sources than the ETCN network. Upon comparing with 1ET2CE and 2ET1CE configurations, we found that the ETCN network detected 1.6% more sources than the 2ET1CE network, and the CECN network detected 1% more sources than the 1ET2CE network. These results suggest that augmenting the ET-CE network with an ET-like (or CE-like) detector in China could yield a higher detection rate compared to integrating a similar detector in Australia. This difference is primarily attributed to variations in antenna response. There are two key aspects to this: Firstly, the geographic positions of the detectors determine the area of the triangle formed by the network and the baseline lengths. A detector in China alters the network geometry, resulting in a larger detector triangle area and different baseline lengths, which enhances the network's triangulation and detection capabilities. Secondly, the orientation of the detector arms affects their

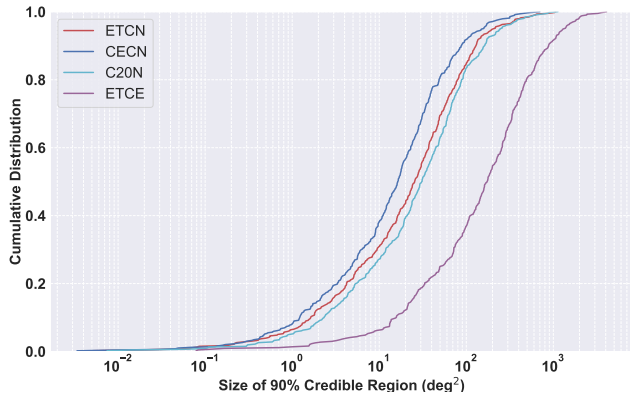


FIG. 3. Cumulative distribution of localization uncertainty for the BNSs in Simulation I. The vertical axis shows the cumulative fraction. The horizontal axis is the size of 90% credible region in deg^2 .

	ETCN	CECN	C20N	ETCE	1ET2CE	2ET1CE
	91.4%	98%	92.2%	87%	97%	89.8%
90%	128.86	87.43	161.51	881.88	56.77	91.79
50%	25.49	16.29	30.82	173.41	12.54	17.57
10%	1.63	1.22	2.33	15.62	1.17	1.37

TABLE II. Values show the 90% credible regions of localization uncertainty in deg^2 for detectable simulated the BNSs in Simulation I. The second row denotes the fraction of detectable sources for each detector network with $\text{SNR} \geq 8$. 90%, 50% and 10% in the first column respectively represents the best localized 90%, 50% and 10% of the detectable sources. The fifth column shows the results for ET-CE network, the sixth column shows the results for ET-CE network plus a CE-like detector in Australia, the last column shows the results for ET-CE network plus an ET-like detector in Australia.

sensitivity to gravitational waves from different sources. A detector in China would have different arm orientations compared to one in Australia, leading to variations in the antenna response and, consequently, differences in sensitivity to sources from various parts of the sky. Therefore, the overall improvement in detection rates is largely due to the differing antenna responses influenced by both the geometric configuration of the network and the orientation of the detector arms.

Figure 2 illustrates the cumulative distribution of signal-to-noise ratio (SNR) for simulated sources detected by networks equipped with detectors in China. The SNR distribution of the CECN network tends to skew towards higher values, contrasting with the ETCN network and C20N network, whose SNR distributions are nearly identical. However, in quantitative terms, the C20N network outperformed the ETCN network by detecting 0.8% more sources overall.

2. Localization performance

Figure 3 illustrates the cumulative distribution of localization uncertainties across various networks. All localization uncertainties in this paper refer to the 90% credible interval of estimated localization uncertainty. Table II further details the localization uncertainty for the top 90%, 50%, and 10% most accurately localized detectable sources, comparing networks with and without a detector in China alongside the ET-CE network for reference. Key observations include: (1) The ET-CE network achieves localization of the top 90% sources within approximately 882 deg^2 . With the addition of a Chinese detector, this uncertainty shrinks dramatically to $\leq 162 \text{ deg}^2$, representing less than one-fifth of the original sky error. (2) In horizontal comparison with networks incorporating an Australian detector, the ETCN network exhibits localization uncertainty approximately 1.4 times greater than the 2ET1CE network for the top 90% of sources. Similarly, the CECN network's uncertainty is approximately 1.54 times greater than that of the 1ET2CE network. This implies that augmenting the ET-CE network with an Australian detector leads to more precise localization for identical BNS mergers compared to integrating a detector in China (It should be noted that in the case of China, the number of sources that meet the detection criteria is relatively higher, which means that some sources with larger localization errors are also included in the statistics. In contrast, for Australia, the sources that are included in the statistics mostly have smaller localization errors. Thus the Chinese networks give better detectability but worse localization than the Australian network.). (3) Among networks featuring a Chinese detector, the CECN network demonstrates the lowest overall localization uncertainty. Specifically, the localization uncertainty of the ETCN (C20N) network is roughly 1.5 (2) times larger than that of the CECN network.

3. Early Warning

If the inspiral signal from a binary neutron star (BNS) merger can attain a sufficiently robust signal-to-noise ratio (SNR) and be localized within a reasonable portion of the sky prior to the actual merger, it opens the possibility of issuing an early warning alert to facilitate observations of any associated electromagnetic counterparts. In our investigation, we operate under the assumption that for an early warning to be issued, the source must satisfy two criteria: firstly, the network SNR for the source must reach a minimum of 8, and secondly, the localization uncertainty should not exceed a predefined sky area (either 30 or 100 deg^2).

The two-dimensional histogram depicting the distribution of time to merger versus the size of the 90% credible region (less than 30 deg^2) when signals have accumulated a network SNR of ≥ 8 for the binary neutron stars

(BNSs) in Simulation I is presented in Figure 4. Among the detector networks, ETCN, CECN, and C20N respectively detect 54%, 67%, and 49% of sources with an SNR of ≥ 8 , successfully localizing them within 30 deg^2 at the time of merger. Notably, the time to merger distribution between CECN and C20N networks exhibits remarkable similarity, with both networks capable of detecting the majority of sources within 3 hours before the merger. Furthermore, ETCN network, overall, demonstrates an earlier detection capability compared to the other two networks. The results pertaining to the maximum allowable region of 100 deg^2 are provided in the appendix.

B. Simulation II: BNS mergers at fixed distances

1. Detection rates

Similarly, with a network SNR threshold set at 8 for detection, both the CECN and C20N networks demonstrated the capability to detect all simulated sources across all tested distances, ranging from 40 Mpc to 1600 Mpc. However, for the ETCN network, three signals at 1600 Mpc remained undetected, while the ET-CE network missed five signals at the same distance.

2. Localization performance

We calculated the localization uncertainty of binary neutron star (BNS) mergers at the time of the merger using tested detector networks. This allowed us to compile percentages of detectable sources that could be localized within 30 deg^2 , 10 deg^2 , 5 deg^2 , and 1 deg^2 for each detector network, providing a comprehensive perspective on their localization abilities. The results are summarized in Table III. We observe that, across various distances and under the same maximum allowable localization uncertainty, the CECN network consistently detects the highest number of sources, with only a few exceptions. Additionally, the ETCN network generally outperforms the C20N network in terms of source detection. Comparing these results with networks incorporating a detector in Australia, we find that the 2ET1CE (1ET2CE) configuration tends to localize more sources than the ETCN (CECN) network within the same maximum allowable region. This suggests that integrating a detector in Australia into the ET-CE network could lead to more accurate localization (at least during the time of merger) for the same binary neutron star (BNS) sources compared to adding a detector in China.

Also, for three tested networks including the detector in China, we show the cumulative distribution of localization uncertainty at the time of merger for the detectable sources (SNR no less than 8) at each fixed distance in Figure 7 of the appendix. Additionally, Table IV provides quantitative values of the corresponding localization uncertainty for the top 90%, 50%, and 10% of best-localized

sources by each network at fixed distances. For example, for the detectable sources at 40 Mpc, ETCN could localize 90% best-localized sources to within 0.019 deg^2 . Take 200 Mpc results in Table IV as an example, we can see that: (1) The ET-CE network can localize 90% of the best-localized sources within 2.175 deg^2 . When an additional detector is added in China to the ET-CE network, the localization error decreases to approximately 10% to 22% of its original value; (2) We observe that, for the top 90% and 50% of best-localized sources, the ETCN (CECN) network consistently exhibits larger localization uncertainty compared to the 2ET1CE (1ET2CE) network. However, for the top 10% of best-localized sources, the ETCN (CECN) network tends to demonstrate comparable or even smaller localization uncertainty than the 2ET1CE (1ET2CE) network. These findings suggest that augmenting the ET-CE network with a detector in Australia generally results in overall smaller localization uncertainty for the majority of sources, while adding a detector in China may lead to better localization for a very small subset of sources compared to Australia; (3) In terms of comparing the three networks featuring detectors in China, an intuitive examination of Figure 7 reveals that the calculated localization uncertainty values by CECN are notably more concentrated on smaller values. Quantitatively, for the top 90% best-localized sources, the localization uncertainty value for CECN is 0.220 deg^2 , representing 45% of the value of ETCN and 52% of the value of C20N. This suggests that CECN exhibits a more accurate localization ability for the same binary neutron star (BNS) sources, followed by C20N, and then ETCN.

3. Early warning

To investigate the capability of tested detector networks for giving early warning alerts, we did some statistics, firstly, for a given sky area, we selected sources that meet two requirements of early warning criteria at the time of merger. Next, based on these selected sources, we obtained the earliest time when the source achieve the early warning criteria. Given respectively the maximum allowable sky area of 1 deg^2 , 5 deg^2 , 10 deg^2 , 30 deg^2 , the cumulative distribution of time to merger (obtained by time of merger - earliest time) when selected BNSs at 200 Mpc achieves the early warning criteria by tested detector networks are shown in Figure 5 (Similar figures for BNSs at other fixed distances can be found in the Appendix.), which shows that in general, the line of ETCN is shifted right the furthest towards higher values, indicating that it achieves the early warning criteria at the earliest time. Additionally, the overall slope of the line of ETCN is steeper than the other two, especially for a larger given sky area (e.g. 30 deg^2). Steeper slopes indicate a tighter range of values and, therefore, lower variability.

One method to read a cumulative distribution in a

		ETCN	CECN	C20N	ETCE	1ET2CE	2ET1CE
200Mpc	30deg ²	100%	100%	100%	100%	100%	100%
	10deg ²	100%	100%	100%	99%	100%	100%
	5deg ²	100%	100%	100%	98%	100%	100%
	1deg ²	98%	97%	96%	72%	100%	100%
400Mpc	30deg ²	100%	100%	100%	99%	100%	100%
	10deg ²	100%	100%	100%	92%	100%	100%
	5deg ²	99%	100%	98%	76%	100%	100%
	1deg ²	74%	92%	69%	10%	95%	89%
800Mpc	30deg ²	100%	100%	100%	84%	100%	100%
	10deg ²	94%	96%	94%	51%	98%	99%
	5deg ²	84%	94%	79%	13%	96%	93%
	1deg ²	40%	54%	35%	0%	64%	53%
1600Mpc	30deg ²	89%	95%	91%	34%	98%	99%
	10deg ²	59%	78%	60%	3%	89%	79%
	5deg ²	46%	59%	42%	0%	70%	58%
	1deg ²	11%	14%	4%	0%	16%	9%

TABLE III. A table showing the fraction of detectable BNSs in Simulation II which can be localized to within 30deg², 10deg², 5deg², and 1deg² at the time of merger with tested networks (ETCN, CECN, C20N), ET-CE network (ETCE), and also ET-CE network together with a detector in Australia (1ET2CE, 2ET1CE).

		ETCN	CECN	C20N	ETCE	1ET2CE	2ET1CE
40Mpc	90%	0.019	0.009	0.017	0.087	0.007	0.010
	50%	0.004	0.002	0.004	0.024	0.001	0.002
	10%	0.001	0.001	0.001	0.010	0.001	0.001
200Mpc	90%	0.486	0.220	0.427	2.175	0.18	0.25
	50%	0.099	0.055	0.106	0.604	0.04	0.06
	10%	0.015	0.013	0.024	0.243	0.01	0.02
400Mpc	90%	1.945	0.880	1.709	8.701	0.72	1.02
	50%	0.396	0.220	0.422	2.416	0.15	0.22
	10%	0.060	0.050	0.096	0.971	0.06	0.06
800Mpc	90%	7.782	3.521	6.836	34.803	2.89	4.07
	50%	1.584	0.881	1.690	9.665	0.60	0.91
	10%	0.241	0.200	0.384	3.885	0.23	0.26
1600Mpc	90%	24.150	14.083	27.345	136.411	10.07	14.65
	50%	5.737	3.524	6.758	36.735	2.30	3.57
	10%	0.931	0.801	1.536	15.318	0.90	1.03

TABLE IV. The 90% credible regions of localization uncertainty in deg² for detectable BNSs in Simulation II. The detectable sources are selected according to SNR larger than 8. Then in detectable sources, values for 90%, 50% and 10% respectively correspond to 90%, 50% and 10% of cumulative distribution, which mean localization uncertainties for best-localized 90%, 50% and 10% of sources. From the third column to the last column, are respectively the results of ETCN network, CECN network, C20N network, ET-CE network (ETCE), ET-CE network together with a CE-like detector in Australia (1ET2CE), ET-CE network together with an ET-like detector in Australia (2ET1CE).

quantitative way is to look up percentiles. For example, for each maximum localization uncertainty case (e.g. 30 deg²), we extract values of time to merger which correspond to respectively 90%, 50%, 10% of for detectable sources at 200Mpc from Figure 5, and the numbers are listed in Table V (the extracted values represent the lower bound of time to merger). Take ETCN and 30 deg² as an example, an early warning can be issued for 90% of the sources as early as ≥ 35 minutes before merger. From this table, we can infer the following: (1) given 30 deg² as the maximum allowable region, for 90% detectable sources, ET-CE network could give alerts at least 3.33 minutes before merger, adding a detector in China raise

this lower limit to 10 minutes, and in some instances, alerts can be released as early as more than 300 minutes before merger; (2) with horizontal contrast with networks including detector in Australia, we can see that given the same maximum allowable sky area, the lower bound of time to merger of ETCN (CECN) is generally larger than 2ET1CE(1ET2CE) network, this means that, based on ET-CE network, adding a detector located in China tends to meet the early warning criteria and release an alert earlier before Australian detector network case; (3) for a relatively large given maximum allowable region, for example, 10 deg² and 30 deg², three detector networks including detector in China, from C20N, CECN, to ETCN,

show an increasing trend of lower limit of time to merger, as intuitively shown in the Figure 5, the three lines are arranged from bottom to top, which means ETCN could achieve the early warning criteria earlier than CECN, and CECN is earlier than C20N. While in 1 deg² case, for 50% detectable sources, the lower limit of time to merger of ETCN and C20N network are both 0, and it is 1.67 minutes for CECN network. This means most detectable sources meet the early warning criteria nearly at the time of merger by ETCN and C20N, while at the same time, most detectable sources achieve the early warning criteria by CECN network before merger and are concentrated in a very narrow range (mainly ~ 1.67 -10 minutes before merger), this is because when BNS is close to merger, the high sensitivity of CE in this frequency range (e.g., 10 Hz - 1000 Hz) enables its detected localization uncertainty to rapidly reach 1 deg² within a few minutes before the merger. And the sensitivity of ET and 20km detector is similar (not better than CE), so the localization uncertainty detected by these two detector networks tends to decrease more slowly to 1 deg², in this case, most detectable sources could be localized to 1 deg² only at the time of merger.

We also did another statistic for localization before merger, as seen in Table VI. Taken 200 Mpc, ETCN network and pre-merger time of 10 minutes as an example, we firstly counted the number of sources of which could be detected with SNR ≥ 8 and localized within 10 deg² at the time of merger, then for these selected sources, we counted the number of sources of which could be detected with SNR ≥ 8 and localized within 100 deg² at 10 minutes before the merger. Finally, the ratio between these two counts are calculated and the values are shown in Table VI as percentages. For BNSs at one selected distance, e.g., 400 Mpc, and by one selected network, we will see that the number corresponding to pre-merger time of 10 min, 20 min, and 30 min is decreasing, which is easy to understand, because the denominator stays the same, and the localization uncertainty is decreasing as time approaches the merger, which means that the localization uncertainty corresponding to 10 min, 20 min, and 30 min is increasing, therefore, the number of sources which meet the criteria in numerator is decreasing. And we can infer the detector network sensitivity from its decreasing rate from 10 min case to 30 min case, usually, when the detector network has better sensitivity during this range, its detected localization uncertainty will decrease quickly with time, thus resulting in more precise source localization. We could find that CECN decreases more quickly than ETCN network, which is because, CECN has better sensitivity especially in 10 Hz - 1000 Hz.

IV. CONCLUSION AND DISCUSSION

In this work, we use Fisher matrix method to estimate the detection rate, localization uncertainty and early

		ETCN	CECN	C20N	ETCE	1ET2CE	2ET1CE
30deg ²	90%	35	20	10	3.33	16.67	18.33
	50%	75	31.67	23.33	18.33	28.33	45
	10%	255	68.33	68.33	68.33	68.33	75
10deg ²	90%	8.33	6.67	1.67	0	6.67	6.67
	50%	36.67	18.33	8.33	3.33	15	28.33
	10%	145	31.67	25	25	30	65
5deg ²	90%	0	3.33	0	0	3.33	1.67
	50%	21.67	11.67	3.33	0	8.33	13.33
	10%	95	21.67	11.67	6.67	18.33	48.33
1deg ²	90%	0	0	0	0	0	0
	50%	0	1.67	0	0	1.67	0
	10%	29.67	6.67	1.67	0	5	11.67

TABLE V. A table showing that given the maximum allowable region of respectively 30deg², 10deg², 5deg², and 1deg², the time to the merger in minutes, 90%, 50%, 10% of the cumulative distribution of time to the merger of detectable events at 200 Mpc by each network.

warning performance of three test networks containing detector in China (ETCN, CECN, C20N) for simulated BNS merger events (two kinds of population: Simulation I, BNS mergers following the delay time distribution; Simulation II, BNS mergers at fixed distances). The results were compared with those obtained from the ET-CE network, and with those obtained from ET-CE plus a detector located in Australia (2ET1CE: ET-CE network + an ET-like detector in Australia; 1ET2CE: ET-CE network + a CE-like detector in Australia).

Firstly, for Simulation I (500 BNS mergers that follow the delay-time distribution with redshift less than 2), using 8 as the network SNR threshold, the ET-CE network can detect 87% of the sources, and could localize the best-localized 90% sources (The following mentioned localization uncertainties are all for best localized 90% sources) within 881 deg². Building upon the ET-CE network, the addition of a detector situated in China enhances the detection capability by at least 4.4% and concurrently reduces localization uncertainty to less than 20% of its original value, reaching within 162 deg². Contrasting these outcomes with the results of incorporating an Australian detector into the ET-CE network, we observe that when an ET-like detector is added to the ET-CE network, placing the detector in China (ETCN) yields a 1.6% increase in detected sources compared to placement in Australia (2ET1CE). However, the localization error also escalates to approximately 140% of the latter scenario. Conversely, with the addition of a CE-like detector to the ET-CE network, placing the detector in China (CECN) results in a 1% increase in detected sources compared to placement in Australia (1ET2CE), with a localization error of approximately 154% of the latter.

Among the three networks containing detectors in China, CECN boasts the highest detection rate, reaching up to 98%, and exhibits the smallest localization error (≤ 87.43 deg²). Conversely, in the other two networks,

	pre-merger time (min)	ETCN	CECN	C20N	ETCE	1ET2CE	2ET1CE
40Mpc	10	100%	100%	100%	100%	100%	100%
	20	100%	100%	100%	100%	100%	100%
	30	100%	100%	100%	100%	100%	100%
200Mpc	10	100%	100%	100%	100%	100%	93%
	20	100%	100%	100%	99%	99%	91%
	30	100%	99%	81%	78.8%	92%	80%
400Mpc	10	100%	100%	91%	75%	97%	48%
	20	100%	90%	57%	46.7%	75%	32%
	30	94%	62%	27%	28.3%	34%	25%
800Mpc	10	81%	77.1%	38.3%	29.4%	67.3%	5.3%
	20	66%	35.4%	6.4%	11.8%	15.3%	0
	30	50%	6.3%	5.3%	9.8%	1.0%	0
1600Mpc	10	44.1%	25.6%	3.33%	66.67%	9.0%	0
	20	30.5%	2.6%	3.33%	66.67%	0%	0
	30	25.4%	2.6%	3.33%	66.67%	0%	0

TABLE VI. Pre-merger localization, number in the table represents $N_{\Delta\Omega < 100\text{deg}^2, t_{\text{pre}}} / N_{\Delta\Omega < 10\text{deg}^2, t_{\text{merger}}}$. The SNR threshold is set to be 8.

C20N achieves a 0.8% higher detection rate than ETCN, albeit with a larger localization uncertainty, approximately 125% of ETCN’s. When considering a maximum allowable sky area, such as 30 deg^2 , the proportions of sources detectable with $\text{SNR} \geq 8$ and localized within 30 deg^2 at the time of merger are 54%, 67%, and 49% for ETCN, CECN, and C20N, respectively. Moreover, for these selected sources, after identifying all instances where they meet the criteria and their corresponding localization uncertainties, we observed that the time distribution of CECN and C20N is similar. In these two networks, the majority of sources reach a localization uncertainty within 30 deg^2 within 1 hour. In contrast, for the ETCN network, most sources are distributed within 2 hours. This indicates that compared with CECN and C20N, the ETCN network accumulates a SNR greater than 8 at an earlier time before the merger, thereby improving the localization accuracy to within 30 deg^2 .

Furthermore, in Simulation II (which focuses on BNS mergers at fixed distances), we simulated 100 sources for each distance. As an illustration, considering a distance of 200 Mpc, the ET-CE network achieves localization of the top 90% best-localized sources within 2.175 deg^2 . Additionally, if the maximum allowable sky area is restricted to 30 deg^2 , the ET-CE network can issue an alert at least 3.3 minutes before the merger for 90% of the detected sources. Building upon the ET-CE network, the addition of a detector located in China leads to a substantial reduction in localization uncertainty, ranging from 10% to 22% of the value observed in the ET-CE network. Moreover, alerts can be issued at least 10 minutes before the merger event, and for select well-localized sources, alerts could even be released more than 300 minutes before the merger. Contrasting these outcomes with the results obtained

from augmenting the ET-CE network with an Australian detector, we observe that when an ET-like detector is added to the ET-CE network, the localization error incurred by placing it in China (ETCN) is approximately 194% of that experienced when placing it in Australia (2ET1CE). However, in terms of early warning, ETCN generally tends to issue alerts earlier than 2ET1CE in most cases. For instance, with a maximum allowable sky area of 30 deg^2 , ETCN can provide alerts at least 35 minutes before the merger for 90% of detections, compared to 18.33 minutes for 2ET1CE. Similarly, when a CE-like detector is added to the ET-CE network, the positioning error of CECN is approximately 122% of that of 1ET2CE, and CECN tends to release alerts earlier than 1ET2CE. Therefore, it suggests that when detectors of the same configuration are added to the ET-CE network, positioning them in Australia could result in more accurate localization, whereas positioning them in China increases the likelihood of issuing an alert earlier. Among the three networks featuring detectors in China, CECN demonstrates the highest localization accuracy, successfully localizing 90% of the best-localized sources at a distance of 200 Mpc within 0.22 deg^2 . In comparison, ETCN exhibits a localization error that is 220% of that of CECN, while C20N’s error is 194% of that of CECN. In terms of early warning, ETCN typically fulfills the early warning conditions earliest, followed by CECN, and then C20N. This order aligns with the sensitivity levels of the three detectors, as the sensitivity of ET is relatively higher in the frequency range of 1 Hz to 10 Hz. Consequently, SNR accumulation can begin earlier with ET, leading to a gradual reduction in localization uncertainty. Conversely, the sensitivity of CE and C20 experiences a notable increase from approximately 10 Hz onwards. Consequently, SNR accumulation and improvements in localization accuracy

commence around this frequency range. Within the 10 Hz to 1000 Hz range, CE exhibits exceptionally high sensitivity, enabling rapid SNR accumulation and reduction in localization error. This facilitates the attainment of the highest localization accuracy at the time of merger.

In conclusion, within the context of third-generation detectors, such as the proposed ET and CE, the addition of a third detector resembling ET or CE can markedly enhance the localization accuracy of BNS mergers. This enhancement can potentially reduce the error to as low as 20% of that observed with ET-CE. Moreover, such additions enable earlier alert releases, a crucial factor for planning subsequent joint GW-EM observations. Integrating an ET-like or CE-like detector into the ET-CE network, when compared to placement in Australia, generally leads to a slight increase in localization error but often results in a modest improvement in detection rate and earlier alert release. Furthermore, among the three networks featuring detectors in China, CECN exhibits the highest detection rate and localization accuracy. However, C20N and ETCN each possess distinct advantages in localization performance for two kinds of simulated BNS mergers. For early warning, ETCN can achieve the criteria earlier thus to release an alert earlier, then followed by CECN, and finally C20N. These results are of great significance for the future cooperative planning of global detectors. In addition, the evaluation of ET-CE plus a detector placed in China in terms of detection rate, localization ability and early warning performance is also of certain reference significance for whether to establish ground-based detector in China in the future.

NSFC (No. 12273058).

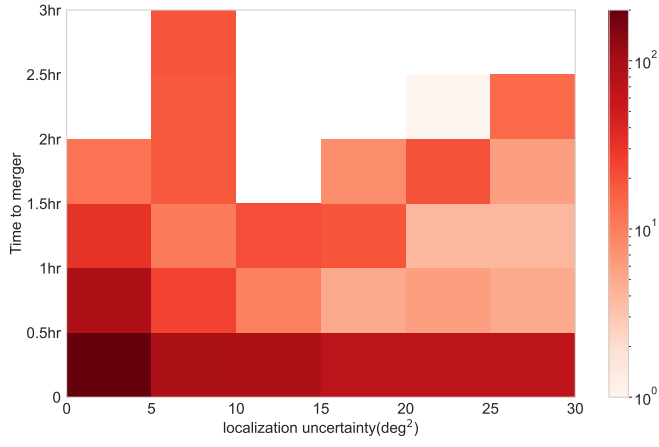
ACKNOWLEDGMENTS

We are grateful to Prof. Mohammadtaher Safarzadeh and Prof. Seyed Alireza Mortazavi for the helpful discussion about the binary neutron star merger rate. We are also grateful for computational resources provided by Cardiff University and funded by an STFC grant supporting UK Involvement in the Operation of Advanced LIGO. This work was supported by the National Natural Science Foundation of China under grant Nos. 11922303, 11920101003. Xilong Fan is supported by the Fundamental Research Funds for the Central Universities (No.2042022kf1182). Y. L is supported by the National Program on Key Research and Development Project through grant No. 2016YFA0400804, and by the National Natural Science Foundation of China with grant No. Y913041V01, and by the Strategic Priority Research Program of the Chinese Academy of Sciences through grant No. XDB23040100. ISH is supported by the Science and Technology Research Council (grant No. ST/V005634/1). LJG is supported by National Key R&D Program of China (No. 2023YFA1607902) and

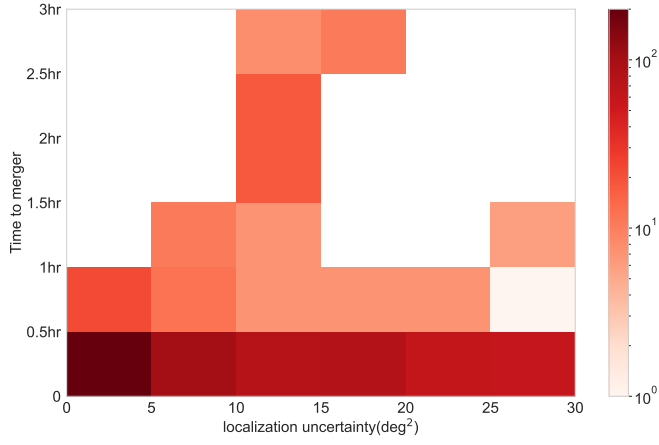
-
- [1] B. P. Abbott, R. Abbott, T. D. Abbott, et al. GW150914: First results from the search for binary black hole coalescence with Advanced LIGO. *Physical Review D*, 93(12):122003, June 2016.
- [2] B. P. Abbott, R. Abbott, T. D. Abbott, et al. GW150914: The Advanced LIGO Detectors in the Era of First Discoveries. *Physical Review Letters*, 116(13):131103, April 2016.
- [3] B. P. Abbott, R. Abbott, T. D. Abbott, et al. Observation of Gravitational Waves from a Binary Black Hole Merger. *Physical Review Letters*, 116(6):061102, February 2016.
- [4] B. P. Abbott, R. Abbott, T. D. Abbott, et al. A gravitational-wave standard siren measurement of the Hubble constant. *Nature*, 551(7678):85–88, November 2017.
- [5] B. P. Abbott, R. Abbott, T. D. Abbott, et al. Exploring the sensitivity of next generation gravitational wave detectors. *Classical and Quantum Gravity*, 34(4):044001, February 2017.
- [6] B. P. Abbott, R. Abbott, T. D. Abbott, et al. Multi-messenger Observations of a Binary Neutron Star Merger. *The Astrophysical Journal Letter*, 848(2):L12, October 2017.
- [7] B. P. Abbott, R. Abbott, T. D. Abbott, et al. Prospects for observing and localizing gravitational-wave transients with Advanced LIGO, Advanced Virgo and KAGRA. *Living Reviews in Relativity*, 23(1):3, September 2020.
- [8] R. Abbott, T. D. Abbott, F. Acernese, et al. GWTC-3: Compact Binary Coalescences Observed by LIGO and Virgo during the Second Part of the Third Observing Run. *Physical Review X*, 13(4):041039, October 2023.
- [9] P. Amaro-Seoane et al. Einstein telescope conceptual design study. Technical Report ET-0106C-10, ET internal note, 2009.
- [10] Vishal Baibhav, Emanuele Berti, Davide Gerosa, Michela Mapelli, Nicola Giacobbo, Yann Bouffanais, and Ugo N. Di Carlo. Gravitational-wave detection rates for compact binaries formed in isolation: LIGO/Virgo O3 and beyond. *Physical Review D*, 100(6):064060, September 2019.
- [11] P. Barriga, D. G. Blair, D. Coward, et al. AIGO: a southern hemisphere detector for the worldwide array of ground-based interferometric gravitational wave detectors. *Classical and Quantum Gravity*, 27(8):084005, April 2010.
- [12] Joshua S. Bloom, Daniel E. Holz, Scott A. Hughes, et al. Astro2010 Decadal Survey Whitepaper: Coordinated Science in the Gravitational and Electromagnetic Skies. *arXiv e-prints*, page arXiv:0902.1527, February 2009.
- [13] Marica Branchesi, Michele Maggiore, David Alonso, Charles Badger, Biswajit Banerjee, et al. Science with the Einstein Telescope: a comparison of different designs. *Journal of Cosmology and Astroparticle Physics*, 2023(7):068, July 2023.
- [14] Kipp Cannon, Romain Cariou, Adrian Chapman, et al. Toward Early-warning Detection of Gravitational Waves from Compact Binary Coalescence. *The Astrophysical Journal*, 748(2):136, April 2012.
- [15] Man Leong Chan, Chris Messenger, Ik Siong Heng, and Martin Hendry. Binary neutron star mergers and third generation detectors: Localization and early warning. *Physical Review D*, 97(12):123014, June 2018.
- [16] Eric Chassande-Mottin, Martin Hendry, Patrick J. Sutton, and Szabolcs Márka. Multimessenger astronomy with the Einstein Telescope. *General Relativity and Gravitation*, 43(2):437–464, February 2011.
- [17] Sheila Dwyer, Daniel Sigg, Stefan W. Ballmer, Lisa Barsotti, Nergis Mavalvala, and Matthew Evans. Gravitational wave detector with cosmological reach. *Physical Review D*, 91(8):082001, April 2015.
- [18] Stephen Fairhurst. Source localization with an advanced gravitational wave detector network. *Classical and Quantum Gravity*, 28(10):105021, May 2011.
- [19] Fermi-LAT Collaboration. Fermi-LAT observations of the LIGO/Virgo event GW170817. *arXiv e-prints*, page arXiv:1710.05450, October 2017.
- [20] Ish Gupta, Chaitanya Afle, K. G. Arun, Ananya Bandopadhyay, Masha Baryakhtar, et al. Characterizing Gravitational Wave Detector Networks: From A³ to Cosmic Explorer. *arXiv e-prints*, page arXiv:2307.10421, July 2023.
- [21] S. Hild, S. Chelkowski, A. Freise, J. Franc, N. Morgado, R. Flaminio, and R. DeSalvo. A xylophone configuration for a third-generation gravitational wave detector. *Classical and Quantum Gravity*, 27(1):015003, January 2010.
- [22] Yi-Ming Hu, Péter Raffai, László Gondán, Ik Siong Heng, Nándor Kelecsényi, Martin Hendry, Zsuzsa Márka, and Szabolcs Márka. Global optimization for future gravitational wave detector sites. *Classical and Quantum Gravity*, 32(10):105010, May 2015.
- [23] Jonah Kanner, Tracy L. Huard, Szabolcs Márka, David C. Murphy, Jennifer Piscionere, Molly Reed, and Peter Shawhan. LOOC UP: locating and observing optical counterparts to gravitational wave bursts. *Classical and Quantum Gravity*, 25(18):184034, September 2008.
- [24] Yufeng Li, Xilong Fan, and Lijun Gou. Constraining the Stochastic Gravitational Wave from String Cosmology with Current and Future High-frequency Detectors. *The Astrophysical Journal*, 887(1):28, December 2019.
- [25] Yufeng Li, Ik Siong Heng, Man Leong Chan, Chris Messenger, and Xilong Fan. Exploring the sky localization and early warning capabilities of third generation gravitational wave detectors in three-detector network configurations. *Physical Review D*, 105(4):043010, February 2022.
- [26] LIGO Scientific Collaboration, J. Aasi, B. P. Abbott, et al. Advanced LIGO. *Classical and Quantum Gravity*, 32(7):074001, April 2015.
- [27] Denis Martynov, Haixing Miao, Huan Yang, Francisco Hernandez Vivanco, Eric Thrane, et al. Exploring the sensitivity of gravitational wave detectors to neutron star physics. *Physical Review D*, 99(10):102004, May 2019.
- [28] Denis Martynov, Haixing Miao, Huan Yang, Francisco Hernandez Vivanco, Eric Thrane, Rory Smith, Paul Lasky, William E. East, Rana Adhikari, Andreas Bauswein, Aidan Brooks, Yanbei Chen, Thomas Corbitt, Andreas Freise, Hartmut Grote, Yuri Levin, Chunnong

- Zhao, and Alberto Vecchio. Exploring the sensitivity of gravitational wave detectors to neutron star physics. *Physical Review D*, 99(10):102004, May 2019.
- [29] M. Punturo, M. Abernathy, F. Acernese, B. Allen, N. Andersson, et al. The Einstein Telescope: a third-generation gravitational wave observatory. *Classical and Quantum Gravity*, 27(19):194002, October 2010.
- [30] M. Punturo, M. Abernathy, F. Acernese, et al. The Einstein Telescope: a third-generation gravitational wave observatory. *Classical and Quantum Gravity*, 27(19):194002, October 2010.
- [31] Tania Regimbau, Thomas Dent, Walter Del Pozzo, Stefanos Giampanis, Tjonnie G. F. Li, et al. Mock data challenge for the Einstein Gravitational-Wave Telescope. *Physical Review D*, 86(12):122001, December 2012.
- [32] David Reitze, Rana X. Adhikari, Stefan Ballmer, Barry Barish, Lisa Barsotti, et al. Cosmic Explorer: The U.S. Contribution to Gravitational-Wave Astronomy beyond LIGO. In *Bulletin of the American Astronomical Society*, volume 51, page 35, September 2019.
- [33] V. Rudenko, S. Andrusenko, D. Krichevskiy, and G. Manucharyan. Optimization of the Euro-Asian network of gravitational detectors for detecting the radiation of collapsing objects. In *Journal of Physics Conference Series*, volume 2081 of *Journal of Physics Conference Series*, page 012011, November 2021.
- [34] Valentin Rudenko, Svetlana Andrusenko, Daniil Krichevskiy, and Gevorg Manucharyan. GW Interferometer Euro-Asian Network: Detection Characteristics for Signals of Known Shape. *Universe*, 6(9):140, September 2020.
- [35] Mohammadtaher Safarzadeh, Edo Berger, Ken K. Y. Ng, Hsin-Yu Chen, Salvatore Vitale, Chris Whittle, and Evan Scannapieco. Measuring the Delay Time Distribution of Binary Neutron Stars. II. Using the Redshift Distribution from Third-generation Gravitational-wave Detectors Network. *The APJL*, 878(1):L13, June 2019.
- [36] B. S. Sathyaprakash, B. F. Schutz, and C. Van Den Broeck. Cosmography with the Einstein Telescope. *Classical and Quantum Gravity*, 27(21):215006, November 2010.
- [37] B. F. Schutz. Determining the Hubble constant from gravitational wave observations. *Nature*, 323(6086):310–311, September 1986.
- [38] Linqing Wen and Yanbei Chen. Geometrical expression for the angular resolution of a network of gravitational-wave detectors. *Physical Review D*, 81(8):082001, April 2010.

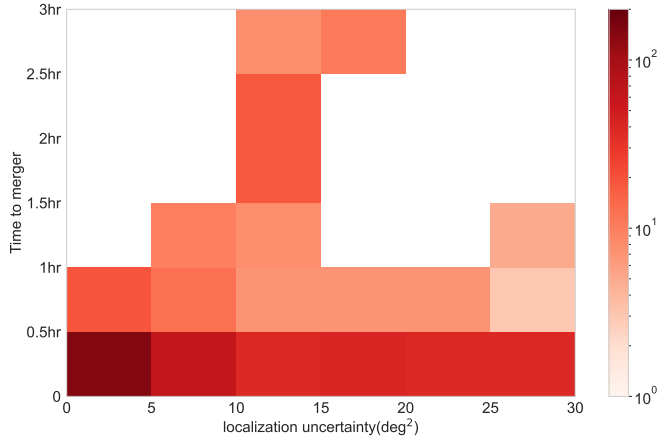
Appendix A: Some extra figures



(a) ETCN network



(b) CECN network



(c) C20N network

FIG. 4. Two-dimensional histograms showing the distributions of the time to merger for the BNSs in Simulation I. The horizontal axis of every subplot is the size of the 90% credible region, and the vertical axis shows the time to merger. The color represents the number of sources that achieve the early warning criteria with the localization requirement being ≤ 30 deg².

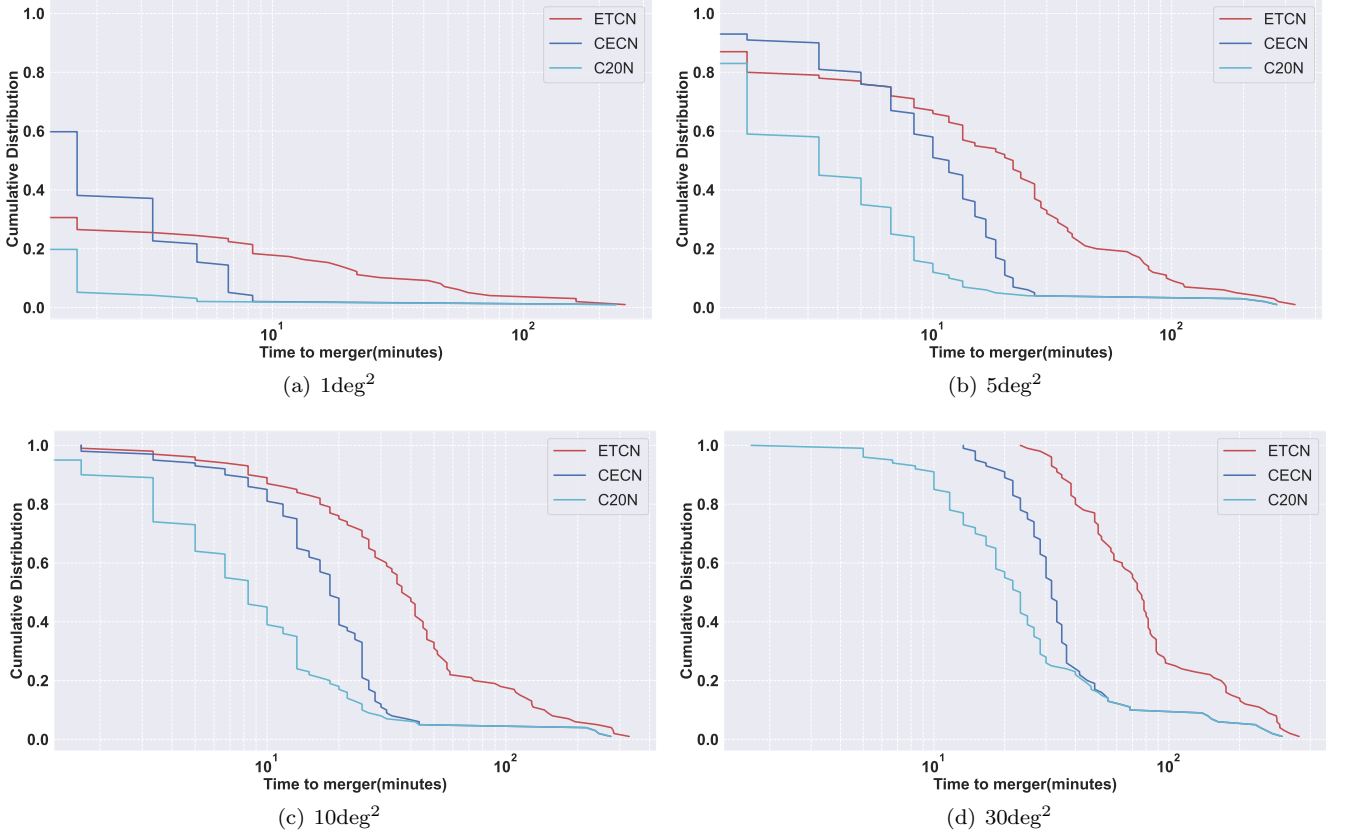


FIG. 5. The cumulative distribution of time to merger for those BNSs at 200 Mpc that achieve the early warning criteria. The x-axis is the time to merger in minutes when the signal meets the localization requirement denoted by deg^2 in subtitle. The y-axis is the cumulative distribution of detectable events that achieve these early warning criteria. All distributions are normalized such that the first bin equals 1.

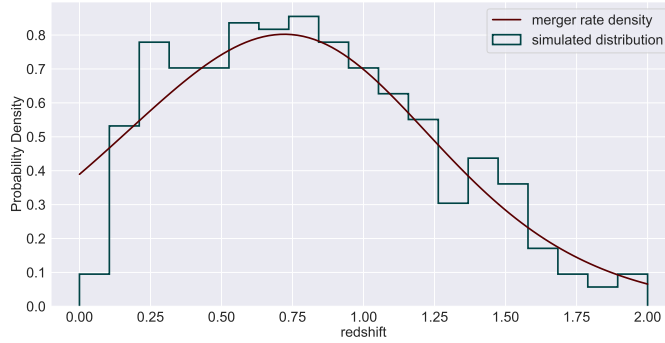


FIG. 6. The distribution of the redshifts of the population of simulated BNS mergers following the delay time distribution. The x-axis represents the redshift and the y-axis represents the probability density. The distribution is normalized such that the area under the curve is 1. The dark brown line is the merger rate density obtained from [35] with $t_{\min} = 1\text{Gyr}$, $\Gamma = -1.5$, and the blue line is the histogram distribution of simulated sources used for later analysis obtained by sampling method from merger rate density.

	Simulation I: BNS population	Simulation II: BNS at fixed distances
source number	500 sources	100 sources respectively at 40 Mpc, 200 Mpc, 400 Mpc, 800 Mpc, 1600 Mpc
source mass (in local frame)	$1.4 M_{\odot} - 1.4 M_{\odot}$	$1.4 M_{\odot} - 1.4 M_{\odot}$
waveform model	TaylorT3	TaylorT3
signal duration	~ 130 hours	~ 130 hours
redshift	follow delay time distribution with maximum ≤ 2	fixed
sky location	randomized	randomized
inclination angle (cosine)	randomized between $(-1,1)$	randomized between $(-1,1)$
polarization angle	randomized between $(0, 2\pi)$	randomized between $(0, 2\pi)$

TABLE VII. Simulated source information. The second column shows the information for simulated BNSs following the delay time distribution shown in Fig. 6 (Simulation I). The last column shows the information for simulated BNSs at fixed distances (Simulation II).

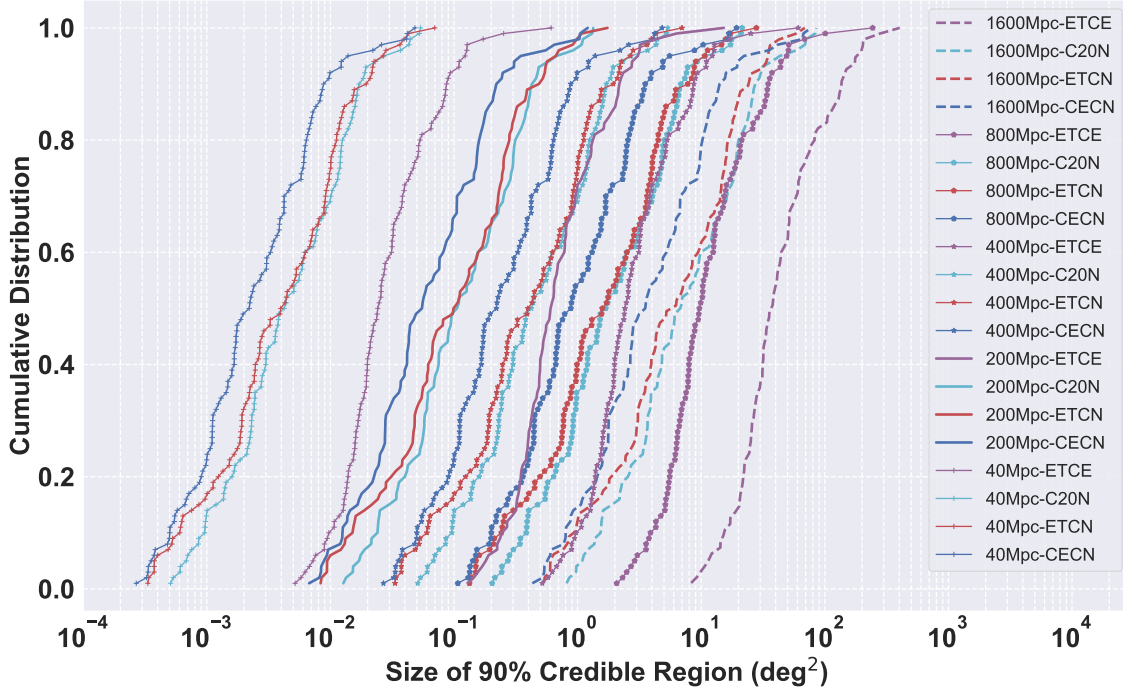


FIG. 7. The cumulative distribution for localization uncertainty of BNS sources at fixed distances.

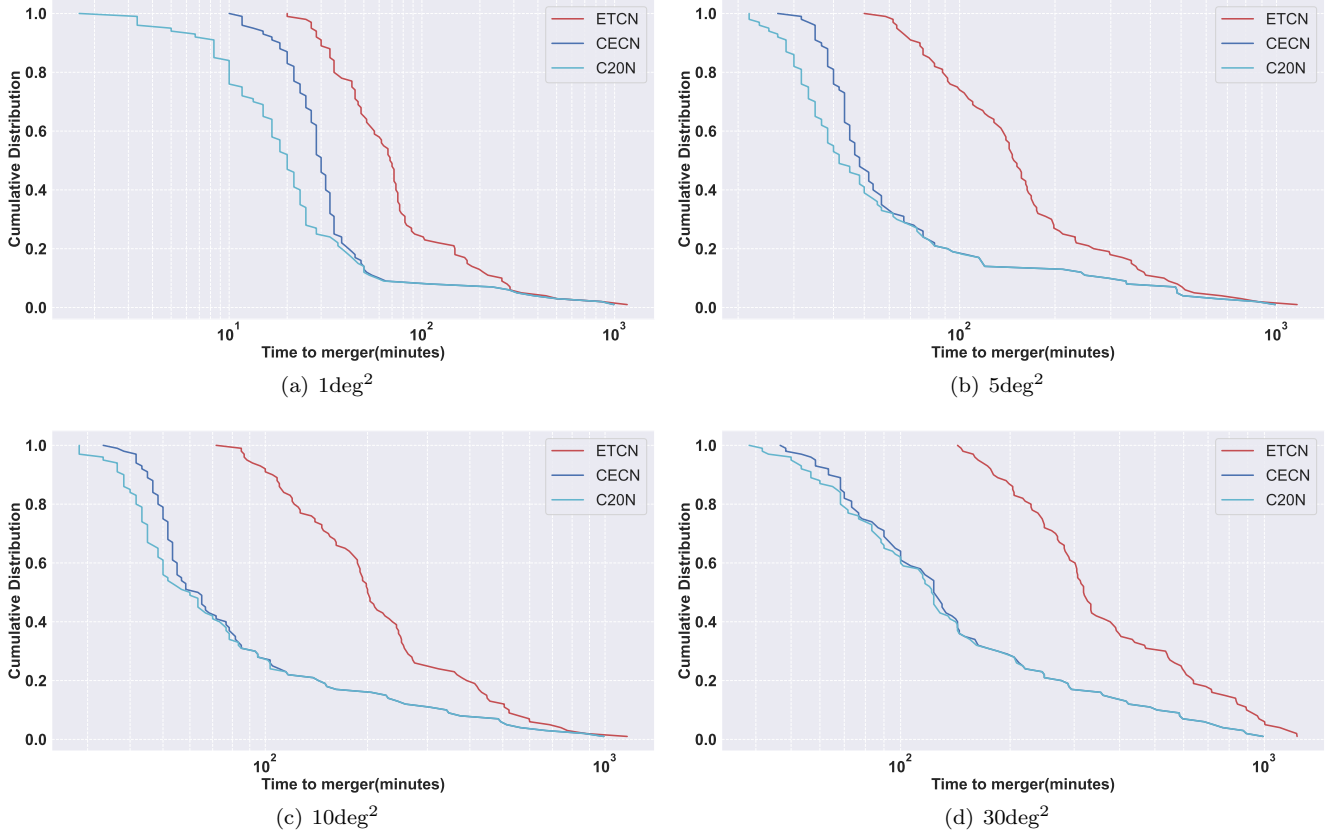


FIG. 8. The cumulative distribution of time to merger for BNSs at 40 Mpc.

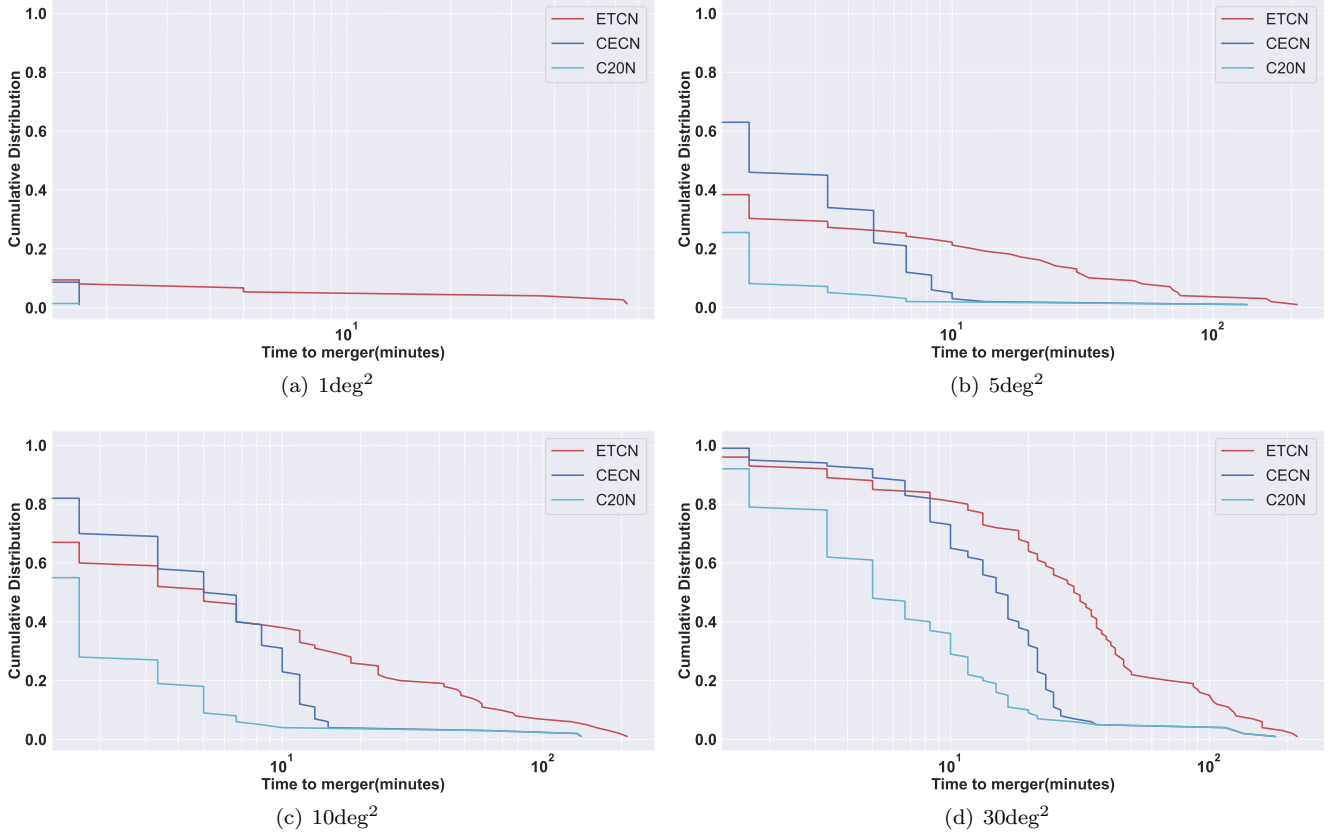


FIG. 9. The cumulative distribution of time to merger for BNSs at 400 Mpc.

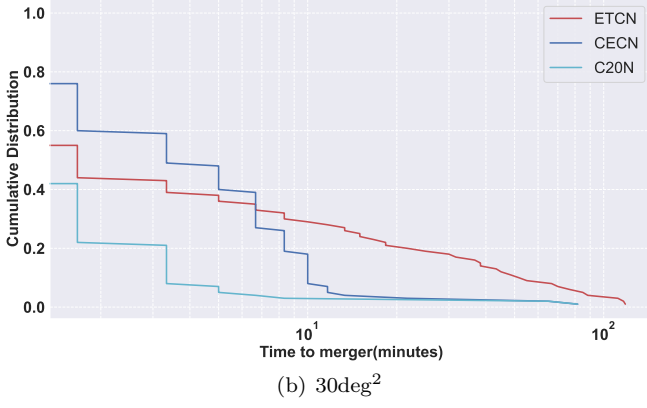
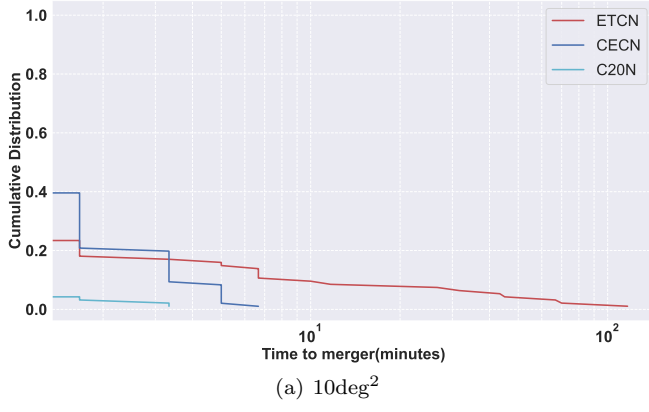


FIG. 10. The cumulative distribution of time to merger for BNSs at 800 Mpc.

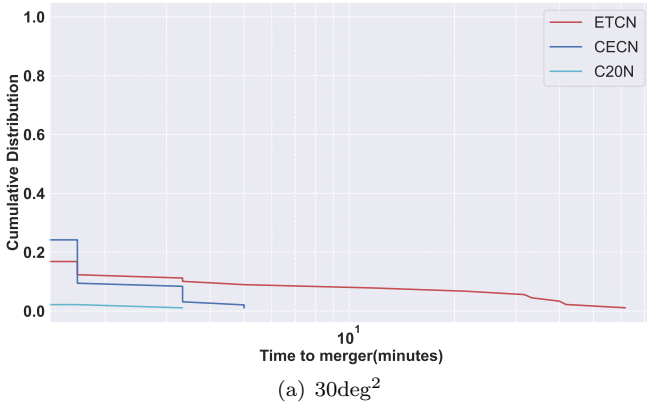
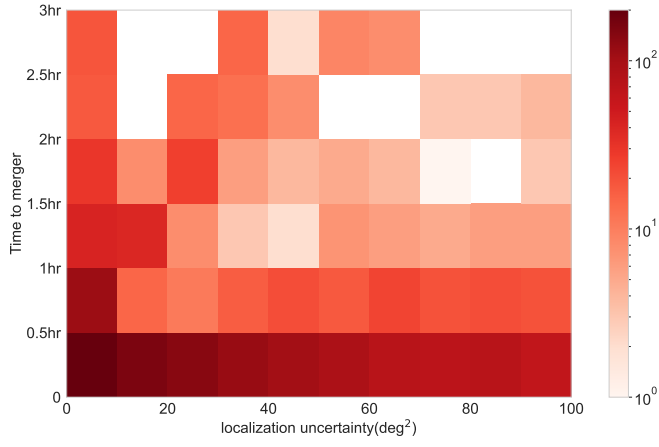
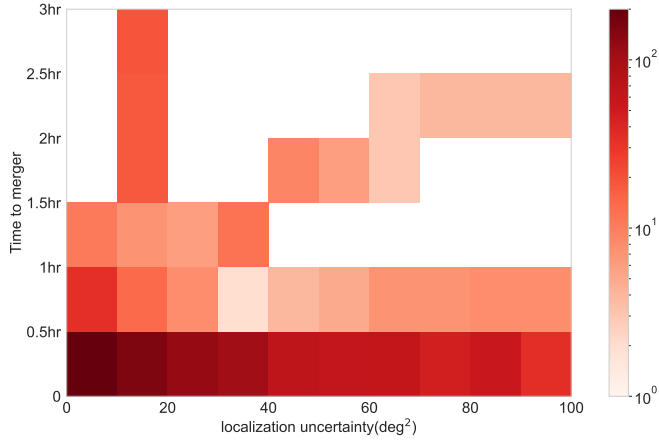


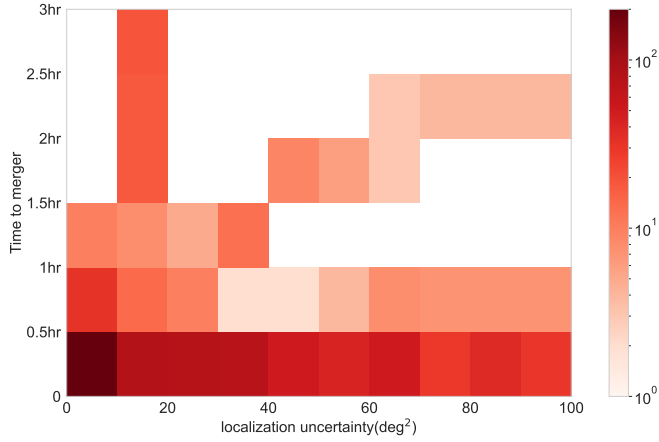
FIG. 11. The cumulative distribution of time to merger for BNSs at 1600 Mpc.



(a) ETCN network



(b) CECN network



(c) C20N network

FIG. 12. Two-dimensional histograms showing the distributions of the time to merger for BNSs in Simulation I. The horizontal axis of every subplot is the size of the 90% credible region, and the vertical axis represents the time to merger. The color represents the number of sources that achieve the early warning criteria with the localization requirement being $\lesssim 100 \text{ deg}^2$.